X-ray photoelectron spectra for single-crystal Ti_{2}O_{3}: Experiment and theory

S. A. Chambers, M. H. Engelhard, L. Wang, T. C. Droubay, M. E. Bowden, M. J. Wahila, N. F. Quackenbush, L. F. J. Piper, Tien-Lin Lee, C. J. Nelin, and P. S. Bagus

Phys. Rev. B **96**, 205143 — Published 27 November 2017

DOI: 10.1103/PhysRevB.96.205143

X-ray photoelectron spectra for single-crystal Ti_2O_3 – experiment and theory

S.A. Chambers[a], M. H. Engelhard[b], L. Wang[b], T.C. Droubay[a], M.E. Bowden[b]
[a]Physical and Computational Sciences Directorate, Pacific Northwest National Laboratory, Richland, WA 99352, USA

[b]Environmental Molecular Sciences Laboratory, Pacific Northwest National Laboratory, Richland, WA 99352, USA

M.J. Wahila, N.F. Quackenbush*, L.F.J. Piper
Department of Physics, Binghamton University, Binghamton, NY 13902, USA
** Present address - Materials Measurement Science Division, National Institute of Standards and Technology, Gaithersburg, Maryland 20899, USA*

Tien-Lin Lee
Diamond Light Source Ltd., Harwell Science and Innovation Campus, Didcot, Oxfordshire OX11 0DE, United Kingdom

C.J. Nelin, P.S. Bagus
Department of Chemistry, University of North Texas, Denton, TX 76203, USA

Abstract

We have measured high-resolution core-level and valence band x-ray photoemission spectra (XPS) for single-crystal Ti_2O_3 cleaved anoxically. The Ti(III) spectra for this lattice are considerably more complex than those measured for Ti(IV)-based oxides due to the presence of a single unpaired electron in the conduction band. This open-shell electron configuration leads to ligand-field split and frequently unresolved multiplets. The Ti 2p and 3p spectra have been calculated using relativistic Dirac-Hartree-Fock (DHF) theory with the sudden approximation for the intensities. Agreement between theory and experiment is excellent for the 3p spectrum, and very good for the 2p spectrum, the primary deficiency being a pair of features not captured by theory for the latter. The spectral line shapes are driven by final-state effects associated with angular momentum coupling of the unpaired valence electron with the core hole, one- and two-electron ligand-to-metal charge transfer (shake) processes accompanying core photoionization, and core-hole screening by conduction band electrons. The first two of these are accurately predicted by DHF theory with a small embedded cluster containing a single Ti cation and six oxygen ligands. The third effect is not predicted using this cluster in which screening of the core-hole from electrons associated with more distant atoms is not possible.

I. Introduction

Transition metal (TM) cations are exceedingly important in the design and synthesis of binary and complex oxides in all forms. The range of stable valences exhibited by TM cations allows for the tailoring of electronic, optical and magnetic properties. Ti is especially important because of sustained, high interest in the various polymorphs of TiO_2, as well as complex oxides, such as $SrTiO_3$, $LaTiO_3$, $GdTiO_3$ and $NdTiO_3$. Polycrystals, nanoscale powders, disordered films, epitaxial heterostructures and bulk single crystals of Ti-containing oxides have been vigorously investigated in recent years, and the level of scientific and technological interest remains strong and diversified. While Ti(IV) is the most stable and ubiquitous cationic form, many important processes result in the reduction of structural Ti(IV) to Ti(III). In contrast, Ti(II) is quite rare. The ability to accurately detect the presence of Ti(III), and not mistaking Ti(III) for a mixture of Ti(III) and Ti(II), is crucial to rigorously characterizing these processes and quantifying the amount of Ti(III) that is present. The latter mistake is easy to make because, as we show below, both the Ti $2p_{3/2}$ and Ti $2p_{1/2}$ manifolds for structural Ti(III) cations contain intense features on the low binding energy sides that could be taken as being due to the presence of Ti(II) if the line shape of Ti(III) is not well understood. We note that the notation Ti(*N*) and is used to describe nominal oxidation states. Herein, the validity of this approximation is investigated. From our analysis of *ab initio* wavefunctions (WF), we show that there is substantial covalent character in the Ti – O bonds, and that nominal oxidation states only reflect the stoichiometry of the material, but not the actual charge states. One reason for the complex character of the Ti 2p and 3p spectra for Ti(III) compared to Ti(IV) is that Ti(III) has an open-shell electron configuration derived from the Ti 3d orbital and the angular momentum coupling of the 2p hole with the open shell leads to multiplets that complicate the spectra. In addition, the influence of covalency on the complex features of core-level x-ray photoelectron spectra (XPS) is revealed.

Since XPS is a widely used spectroscopy for determining the properties of solids, specifically TM cation valences in the near-surface region of oxides, the correct interpretation of TM cation core-level XPS is a major focus of this paper. Furthermore, the depth sensitivity of XPS can be increased using hard x-ray XPS (HAXPES), which allows the probe depth to be extended from a few nm, as is common in the use of soft x-ray synchrotrons and lab-based x-ray sources, to a few tens of nm by increasing the accessible kinetic energy range. For XPS at any energy, understanding the complex lines shapes that result from coupling the core hole to unpaired valence *d* electrons, as well as many-body charge transfer effects, is essential for accurate interpretation of TM cation spectra. For many elements and compounds, the shifts in XPS binding energies (BE) can be directly related to properties of the initial state charge distributions. For example, core binding energies typically increase with increasing valence, a well-known example being the different valences of Si in thin, amorphous SiO_2 films on Si single crystals [1]. Furthermore, the changes in interatomic distances between small metal particles and bulk metal contributes significantly to the BE shifts in these particles, since these changes in distance directly affect the charge distribution [2-3]. However, for ionic compounds, especially TM oxides and halides, multiplet splitting and charge transfer (shake) processes can redistribute intensity over ranges of binding energy comparable to those spanned by changes in valence, making it difficult to disentangle these three effects. Some form of theoretical modeling of core-level line shapes is essential. Due to the complexity of these interactions, first-principles calculations without adjustable parameters are often best for the most rigorous and accurate simulation of core-level spectra; see, for example, comparisons between *ab initio* and Anderson model semi-empirical studies of the core-level spectra [4].

Ti_2O_3 is a simple binary oxide containing Ti(III). It exhibits a corundum-like crystal structure of space group $R\bar{3}c$ [5]. It is also a small-gap ($E_g = 0.13$ eV), antiferromagnetic Mott-Peierls insulator that undergoes a broad transition to a metallic state between 400K and 500K, which is below the Néel temperature (660K) [6-7]. The experimental gap is well reproduced theoretically using the modified Becke-Johnson exchange correlation potential [8]. Atom projected densities of states show that the deeply bound portion of the valence band (VB) is an admixture of O 2p and Ti 3d, with the majority being O 2p. These calculations also reveal a high-lying VB feature just below the Fermi level that is primarily Ti $3d_{Z2}$ in character in which the single unpaired electron formally associated with Ti(III) resides. There is relatively little in the literature on core-level photoelectron spectra from phase-pure Ti(III)-containing materials. Yan *et al.* [7] measured Ti 2p spectra for Ti_2O_3 nanopowders. Kurtz and Henrich [9] published core-level spectra for UHV-cleaved single-crystal Ti_2O_3. In both cases, the spectra were measured with relatively low energy resolution. As a result, the Ti 2p spin-orbit manifold is exceedingly broad and contains many unresolved features, precluding accurate measurement and assignment of the various peaks. It is therefore of scientific and technological interest to measure high-energy resolution core-level spectra for phase-pure single crystal Ti_2O_3 under conditions that preclude surface oxidation. Such spectra can be used to positively identify Ti(III) when it is formed in, for example, charge transfer or unintentional doping processes at interfaces of oxides containing Ti. A well-known example is the onset of conductivity and two-dimensional electron gas (2DEG) formation in undoped $SrTiO_3(001)$ when thin layers of incompletely oxidized γ-Al_2O_3 are deposited [10]. Unreacted Al atoms in the film steal oxygen from the STO due to the large thermodynamic drive to form Al_2O_3. A broad shoulder appears on the low binding energy side of the normally sharp Ti $2p_{3/2}$ peak that is suspected to be due to the presence of Ti(III). Another example is what occurs when epitaxial films of $NdTiO_3(001)$ (NTO) are exposed to air [11]. XPS data and first-principles calculations reveal that oxygen is absorbed, leading to a transfer of Ti 3d valence electrons from structural Ti(III) cations to interstitial O_2 in the lattice. This in turns leads to the presence of both Ti(III) and Ti(IV) in the near-surface region.

In this paper, we describe a joint experimental and theoretical investigation of XPS for single-crystal Ti_2O_3 where our focus is on the Ti 2p and 3p core-level spectra. We present high-energy resolution XPS and HAXPES spectra for specimens cleaved in an oxygen-free environment, along with *ab initio* relativistic cluster calculations of core-level line shapes which include the relevant many-body physics with no adjustable parameters; a general description of our theoretical and computational approach is published elsewhere [4, 12-13]. Our analysis shows the importance of two different kinds of many body effects for the complex Ti 2p and 3p spectra. These are angular momentum coupling (AMC) of the core hole to the unpaired valence *d* electron associated with Ti(III), and excitations from fully occupied predominantly O 2p orbitals that have covalent bonding character with Ti 3d into partially occupied predominantly Ti 3d orbitals that have covalent anti-bonding character with O 2p. These excitations can be described as shake processes since they involve ionization of a core level and excitation from a bonding valence to an anti-bonding level; they have also been described as charge transfer (CT) satellites [4]. In this connection, we also provide quantitative evidence for the covalent character of the Ti-O bonds in Ti_2O_3 and how covalency is involved in screening the core hole. Finally, we suggest that limitations in our modelling of the Ti 2p spectrum may be due to a type of nonlocal screening that involves the free carriers in the conduction band (CB) of Ti_2O_3.

II. Experimental and Modeling Details

The single crystals of Ti_2O_3 used in this experiment were synthesized by T. Reed at MIT Lincoln Lab decades ago by first combining high-purity TiO_2 and TiH_4, then calcining the mixture at 1000^{o}C in vacuum, and finally melting and crystalizing in a crucible [14-15]. X-ray diffraction data were collected at PNNL using a Rigaku D/Max Rapid II micro diffraction system with a rotating Cr target (λ = 2.2910 Å) operated at 35 kV and 25 mA. A parallel X-ray beam collimated to 300 μm diameter was directed onto the specimen that was inclined at 45^{o} about the beam axis and 25^{o} about an axis vertically perpendicular to the beam. Diffracted intensities were recorded on a large 2D image plate and the instrument software used to obtain the direction of the scattering vector relative to the sample surface for any (x,y) coordinate of the image plate. A series of measurements were taken with the sample rotated at 2^{o} increments about an axis perpendicular to its surface so that pole figures of any observable diffraction peak could be constructed from the direction and intensity of the scattering vector.

Electrical transport data were measured at PNNL using a Quantum Design Physical Properties Measurement System (PPMS). Prior to applying In contacts for resistivity and Hall measurements, the surface was scraped on the bench to remove the surface layer of TiO_2 that results from oxidation of Ti_2O_3 in air.

Photoemission measurements utilized monochromatic AlKα x-rays at PNNL, as well as hard x-rays at the Diamond Light Source (UK). The use of x-ray energies ranging from 1.5 keV to 6 keV enabled probing the near-surface as well as deeper regions to determine the depth to which oxidation occurs when anoxically cleaved Ti_2O_3 is exposed to oxygen. Spectra measured at PNNL utilized a PHI Quantera Scanning X-ray Microprobe with an energy resolution of ~0.5 eV. The binding energy scale was calibrated using the Cu $2p_{3/2}$ (932.62 eV) and Au $4f_{7/2}$ (83.96 eV) peaks from clean metal foils. HAXPES measurements were performed at the I09 Surface and Interface Structural Analysis beamline of the Diamond Light Source in the UK. The beamline makes use of two canted undulators that enable photon energies ranging from 100 eV to 20 keV. The hard x-ray branch used for HAXPES measurements enables a photon energy range from 2.1 to 20 keV. The photon beam was monochromated using a channel-cut Si(004) crystal following a Si(111) double-crystal monochromator. Photoelectron spectra were energy resolved and measured using a VG Scienta EW4000 high-energy analyzer with a 30° acceptance angle. Measurements were performed at hν = ~6 keV with an overall energy resolution of < 250 meV. The binding energy scale was calibrated using the Au 4f and Au 4p peak positions, along with the Fermi edge of a gold foil.

Specimens were cleaved either under vacuum in an antechamber appended to the XPS system at PNNL or in a anoxic glovebox, immediately followed by transfer to a vacuum suitcase which could then be connected to the HAXPES end station at Diamond. There was no attempt to cleave along any particular orientation as the bulk crystals were irregularly shaped. However, the cleaved surfaces were mirror-like under an optical microscope, suggesting that cleavage occurred along a single orientation. Avoiding air exposure for the freshly cleaved surfaces was essential because of the extreme instability of structural Ti(III) in the presence of oxygen. Indeed, it was found that Ti(III) in the near-surface region of a freshly cleaved specimen underwent extensive oxidation to Ti(IV) in a matter of minutes in air. Spectra collected at Diamond were taken at room temperature and at ~600K after several hours of outgassing at lower temperatures, allowing the effects of the metal-to-insulator transition (MIT) on the spectra to be determined.

A cluster with a central Ti atom and six nearest O neighbors was used to model the spectra for Ti_2O_3; a schematic representation of the cluster is shown in Fig. 1 The cluster was embedded in several shells of point charges with the nominal ionicities of Ti and O to represent the Madelung potential. The rhombohedral geometry of the Ti_2O_3 crystal was used for the coordinates of the atoms and point charges.

Fully relativistic *ab initio* calculations were carried out using the Dirac-Coulomb Hamiltonian where standard approximations for the Hamiltonian, including approximations for the class of integrals connecting the small components of the relativistic spinors were used [16]. We follow standard usage and describe our theoretical methodology as ligand field theory to distinguish it from crystal field theory. The essential element of this distinction is that the covalent mixing, or hybridization, of metal and oxygen orbitals is explicitly taken into account in ligand field theory, but not in crystal field theory. An excellent description of the distinction of ligand and crystal field theories is given in Ref. [17] where a discussion of the historical development of these methods is also given.

From our extensive prior work with the ligand field wavefunctions for minimal clusters like the embedded TiO_6 cluster used here, it is known that the cluster can represent several important features that contribute to the spectra; see, for example, Ref. [4] and references therein. In particular, the multiplets arising from the AMC of the open shell electrons and the ligand field and spin-orbit splittings are reasonably well described. This conclusion is supported by studies with larger clusters where some of the embedding point charges were replaced with extended ions [18-21]. However, there are physical effects related to the interaction between Ti cations that are not included in the embedded TiO_6 cluster model; see the example, Refs. [22-23]. Indeed, features that are missing from comparison of the theoretically predicted Ti 2p XPS with experiment are discussed in terms of possible limitations of the cluster model that was used. However, investigation of extended cluster models is outside the scope of the present paper.

The solution of the many-electron Hamiltonian was carried out in two stages; first variationally optimized spinors, four component spin orbitals, were determined and the many-electron WFs were calculated. This division is essential for open shell systems where the AMC of the open shell electrons normally precludes the use of single determinant WFs [4, 16].The variationally optimized four component spin orbitals were determined by solving the Dirac-Hartree-Fock (DHF) equations for the average of initial and final core-ionized configurations.[16]. Within the formalism used, there are two different sets of orbitals; one set is for the initial-state configuration with filled core shells, denoted $\varphi_i(I)$, and a second set for the final-state configurations with a core hole, denoted $\varphi_i(F)$. While the two orbital sets are orthogonal within themselves, they are not orthogonal to each other; specifically,

$$< \varphi_i(I)|\varphi_i(F) > \neq \delta_{ij} \qquad (1)$$

The different orbitals for the initial and final core hole configurations are needed to properly take into account the screening in response to the presence of the core hole [4]. *N*-electron Slater determinants [24] were then formed as anti-symmetrized products of *N* of these spinors where the K^{th} determinant is denoted Φ_K. Total *N*-electron WFs, denoted Ψ_J, are obtained by diagonalizing the Hamiltonian connecting the various determinants,

$$\Psi_J = \sum_K C_{JK} \Phi_K \qquad (2)$$

where Ψ_J is described as a configuration interaction (CI) WF; see, for example Refs. [16, 24]. The Hamiltonian is solved for the full set of states possible for the number of determinants used. For the final states, it is essential to solve for a large set of states since these represent main and satellite peaks in the spectra [4]. The active orbital spaces are chosen so that the determinants included in Eq.(2) are sufficient to provide many-body solutions, Ψ_J, that include AMC and other many-body effects. The details of the choices of orbital and determinantal active spaces are given later when we describe the theoretical analysis of specific core-level spectra. The active orbital spaces are chosen so that the determinants included in Eq. (2) are sufficient to provide many-body solutions, Ψ_J, that include AMC and other many-body effects. The details of the choices of orbital and determinantal active spaces are given later when we describe the theoretical analysis of specific core-level spectra. These CI WFs treat scalar relativistic effects, spin-orbit splittings, ligand-field splittings, and open-shell AMC on an equal footing [4]. We have also used new methods of analysis of the orbitals and the CI WFs, especially to characterize the extent and importance of the covalent interactions between the Ti 3d and O 2p [12, 25]. These methods are discussed in Sec. IIID where the covalent character of the initial and final core-hole states is presented.

The XPS intensities were obtained using the sudden approximation [4, 26] where full account was taken of the fact that different sets of spinors are used for the initial and final states. The fact that different orbitals are used for the initial- and final-state WFs means that determinants over these orbitals must be evaluated [27]. This is done using a cofactor analysis [28-29]. In order to make a meaningful comparison with experiment, the calculated core-level intensities were broadened with a Voigt convolution of Gaussian and Lorentzian functions [30]. The Gaussian broadening represents instrumental resolution and excitation to vibrationally excited states [4, 31] while the Lorentzian broadening represents the core-hole lifetime.

The intent behind this brief description of the theoretical methodology is to provide a background for the physical basis of the approximations used to describe the many-body effects included in the theoretical description of the Ti_2O_3 XPS presented in Sec. III below. Further details of the methods are described elsewhere; see Refs. [4, 12-13] and references therein. The spinors and total *N*-electron WFs were determined using the Dirac08 program system [32]. The XPS intensities were determined with programs in the CLIPS program system [33] interfaced to accept orbital and WF information from the Dirac08 calculations.

III. Results and Discussion

A. Physical Characterization of Ti_2O_3

X-ray diffraction shows that the specimens consist of single-crystal Ti_2O_3 corundum with the expected bulk lattice parameters. Pole figures of the Ti_2O_3 $(11\bar{2}6)$ and $(02\bar{2}4)$ diffraction peaks are shown in Fig. 2. The figure shows the expected six-fold and three-fold symmetries for these Bragg reflections, confirming that the sample is a single-crystal. The radial inclinations of ca.

41° and 57° for the $(11\bar{2}6)$ and $(02\bar{2}4)$ peaks also show that the sample surface is approximately parallel to (0001).

Resistivity and Hall measurements are shown in Figs. 3a&b, respectively. The $\rho(T)$ data indicate semiconducting behavior, with an activation of conduction of 0.027 eV in the vicinity of room temperature, as extracted from an Arrhenius plot. The down-tick in ρ as T approaches 400K is presumably the start of the broad MIT between 400K and 500K [6-7]. The majority carriers are electrons, and the carrier concentration at 300K is 1.28×10^{20} cm^{-3}, as determined from the slope of the Hall plot.

B. Core and valence band spectra

We first demonstrate the extreme sensitivity of Ti_2O_3 to oxygen by showing in Fig. 4 Ti 2p spectra measured at room temperature with AlKα x-rays for a anoxically cleaved crystals of Ti_2O_3 and TiO_2 rutile single crystals, along with the effects of air exposure of the former. The primary spin-orbit (SO) features are centered at 455-459 eV (j = 3/2) and 461- 465 eV (j = ½). Shake-up satellites are seen at 471-473 eV and ~477 eV. The SO features are sharp singlets in TiO_2 and complex multiplets in Ti_2O_3. These substantial differences are due to AMC between the 2p hole and the single, unpaired 3d electron present in the valence band of Ti_2O_3, as discussed in more detail below. The TiO_2 line shape does not change upon air exposure whereas the Ti_2O_3 line shape changes substantially. As little as 60 seconds of air exposure significantly reduces the intensities of the lower binding energy features uniquely found in the Ti_2O_3 spectrum. Additional days of air exposure result in only a modest diminution of the Ti(III) features. These results are consistent with rapid oxidation of Ti(III) in the near-surface region to Ti(IV), followed by kinetically limited oxidation of Ti(III) deeper below the surface, but still within the XPS probe depth.

Next we show in Figs. 5 & 6 the valence band (VB) and several core-level spectra for Ti_2O_3 measured with hard x-rays above and below the MIT. The electronic phase transition results in a ~0.5 eV decrease in binding energy for both major VB components (Fig. 5). Additionally, the density of states at the Fermi level increases approximately five-fold at the higher temperature. Although our PPMS cannot operate above 400K, precluding measurement at 600K, we estimate the carrier density at 600K to be ~6×10^{20} cm^{-3} based on this five-fold increase. This higher carrier density has a marked effect on the Ti core-level line shapes, as seen in Fig. 6.

Fig. 6 reveals that there are clear intensity increases and binding energy decreases on the low-energy sides of all Ti core-level peaks in going through the MIT, but not so for the O 2s peak. These results are suggestive of strong screening of the various core holes on Ti by free carriers in the largely Ti 3d-derived CB, the extent of which increases with carrier density. However, both AMC and CT satellites are also expected to add to the complexity of the core-level spectra, and our goal is to disentangle these three effects. The AMC between a core hole in either the Ti 2p or 3p orbital and an unpaired electron in the Ti 3d-derived CB leads to 60 possible final states. This follows because there are 6 ways to remove a 2p or 3p electron from the closed shell and 10 ways to place an electron in the 3d shell which results in 60 determinants corresponding to the $n\mathrm{p}^5 n\mathrm{d}^1$ configuration. Since the final states are linear combinations of these 60 determinants, they may have non-zero spectral weight. As we show below, these states lead to unresolved multiplets in the measured spectrum. When other many body effects are taken into account the number of final states increases dramatically and can be more than two orders of magnitude larger. An important consequence is that many individual final states can, and do, contribute to the overall spectrum and, hence, must be taken into account to obtain an accurate description. However, the covalent character of the orbitals used to generate the determinants that represent different many-body effects is, in fact, a good indicator of whether a given determinant will have significant spectral weight. The covalent character of the Ti-O bond is also a major contributor to the screening of the various core holes. This topic is discussed in relation to possible limitations of the embedded TiO_6 cluster model which has been used, in section IIID.

C. Analysis of the Ti 2p and 3p spectra

In using XPS to characterize oxides containing Ti, the Ti 2p and 3p core levels are most commonly utilized. The 2p is arguably more useful because it has a higher cross section than the 3p, and because it is readily accessible using lab x-ray sources, unlike the Ti 1s. For Ti(IV), the line shape is rather simple because there are no open-shell electrons and, hence, there is only a single multiplet arising from ionization of each of the Ti 2p electrons. CT satellites occur, but there is no AMC. As a result, the Ti 2p spectrum consists of four well-separated features: $j = 3/2$ main peak and satellite, and $j = 1/2$ main peak and satellite. In contrast, the Ti 2p manifold for Ti(III) is considerably more complex. It consists of a single unresolved doublet and a shake-up satellite ~14 eV to higher binding energy. In what follows, we show that solution of the DHF equation accurately reproduces all features, with the exception of what we tentatively assign as well-screened final states by CB electrons in the Ti 2p spectrum. For the Ti 3p manifold of Ti(III), the splittings of the final-state multiplets are smaller in magnitude, especially those for spin-orbit interaction. This results in a very broad leading peak due to many unresolved multiplets and a low-intensity feature at a binding energy of ~13 eV above the main peak, the latter having contributions from AMC and shake excitations.

As briefly described in the section on Experimental and Modeling details, we used a TiO_6 cluster embedded within an array of point charges in a corundum lattice with structural parameters corresponding to bulk Ti_2O_3. Configuration interaction (CI) wavefunctions were used to treat several distinct sets of many-body effects. The first kind of these is the AMC of the open core shell (Ti 2p or 3p) with the dominantly Ti 3d open valence shell. We describe this as a many-body effect because the AMC multiplets cannot in general be represented by a single determinant [24]. In this treatment, we allow the Ti *n*p hole to be placed in any of the six p shell orbitals, and the open-shell electron to be placed in any of the 10 dominantly 3d open-shell orbitals (see Tables I and II), leading to a CI which involves the mixing of 60 determinants. The second kind involves redistribution of the electrons that occupy the Ti 3s, 3p, and 3d shells in different ways over the 18 3s, 3p, and 3d orbitals. For example for the Ti 2p-hole, there will be 9 electrons, from $3s^2 3p^6 3d^1$ distributed over the 3s, 3p, and 3d orbitals. This choice is made because there are atomic many body effects that have the potential to lead to a strong mixing of these excitations with the 60 determinants from AMC coupling [4]. The kinds of excitations made are restricted based on considerations of the atomic parity of these shells such that the odd "atomic" parity of the AMC determinants is maintained. Although parity is broken in the rhombohedral geometry of Ti_2O_3, it is a reasonable approximation for these shallow core orbitals. The third kind is the excitation of a single electron from the dominantly O 2p orbitals, especially those that have significant covalent mixing with Ti 3d, into the dominantly 3d open-shell orbitals. Finally, the fourth kind is excitation of two electrons from the dominantly O 2p orbitals into the dominantly 3d open-shell orbitals. The determinants in sets associated with effects three and four represent shake excitations where one or two valence electrons are promoted from the closed-shell orbitals that can have bonding character between O 2p and Ti 3d into the open-shell orbitals that have anti-bonding character [4]. For these two classes of excitations, the orbitals from which excitations were made and into which the excited electrons were placed were restricted to those orbitals with the largest extent of covalent character, since these are expected to lead to final states with the largest intensities. This was done to maintain a computationally manageable number of determinants in the CI calculations.

In order to determine theoretical core-level spectra, we used the sudden approximation. [4, 26] The spin-orbit and rhombohedral crystal field splittings lead to 6 low lying electronic initial states for the $3d^5$ open shell of Ti; these splittings are discussed in detail when the electronic structure of Ti_2O_3 is considered in section III.D. We assume that the initial states are well described with a Boltzmann distribution at room temperature over the ligand and spin-orbit split initial states (see Table I). The calculated intensities were Voigt broadened with a Lorentzian to represent core-hole lifetime and a Gaussian to represent experimental resolution and other broadening effects, including Franck-Condon vibrational excitations [30-31]. Dual Voigt broadening was carried out incorporating the difference in core-hole life times for the j = 3/2 and j = 1/2 spin-orbit states due to the Coster-Kronig decay channel available only to the j = 1/2 state. The associated widths are 3.0 eV full width at half-maximum (FWHM) for the Gaussian components and 0.75 eV and 0.25 eV FWHM for the Lorentzian components of $2p_{1/2}$ and $2p_{3/2}$, respectively. The Lorentzian lifetime broadenings were based on our analysis of the Ti(IV) XPS spectra [34] and the Gaussian broadenings were selected to provide the best fit to the experimental XPS. The analogous numbers for the Ti 3p XPS are 2.5 eV for the Gaussian and 1.0 eV (0.5 eV) for Lorentzian on $3p_{1/2}$ ($3p_{3/2}$).

In Fig. 7, we show the progression of the predicted Ti 3p spectrum as different many body effects are included. For each case, the number of determinants in the CI Hamiltonian is shown. In addition to the total spectra shown as a solid line where all theoretical contributions are summed, the contributions from individual final states with the largest intensities are also shown.

The zero of the relative binding energies (E_{rel}) is taken as the lowest energy state for the np hole configuration. The experimental spectra are shown as dotted lines in the figure and are shifted so that the theoretical and experimental maxima are at the same E_{rel}. As seen in Fig. 7a, when only AMC many-body effects are included, the theoretical spectrum is too broad in the first peak and does not have sufficient intensity for the peak at $E_{\mathrm{rel}} = \sim 15$ eV. All of these peaks arise entirely from AMC, including the intensity at $E_{\mathrm{rel}} = \sim 15$ eV, which is due to the low-spin coupling of the open Ti 3p and 3d shells [35-36]. From the underlying curves in Fig. 7 it is clear that many individual final states contribute to the total spectrum. In particular, the broad leading peak contains intensity from several unresolved multiplets. When the intra-atomic many body effects of the second kind are added (Fig. 7b), intensity is shifted from the main peak to the feature at E_{rel} = ~15 eV. Although agreement with experiment is slightly better, this feature still has significantly lower intensity than that measured. When single and double inter-atomic shake excitations are included (Figs. 7c & d), the main changes are in the peak at E_{rel} = ~15 eV peak; the leading peak is not significantly affected. Indeed, at this point, agreement between theory and experiment is excellent. The broad leading edge feature is dominated by AMC with perturbation from atomic near degeneracy many-body effects due to moving electrons within the Ti 3s, 3p, and 3d shells. The feature at E_{rel} = ~15 eV has some contribution from AMC and other atomic many-body effects. It also has important contributions from inter-atomic shake in which electrons are excited from closed-shell O 2p + Ti 3d bonding orbitals into open-shell Ti 3d + O 2p anti-bonding orbitals.

In Fig. 8, we show a similar progression for the predicted Ti 2p spectra as different sets of many body effects are included. When only AMC effects are considered (Fig. 8a), the theory predicts a spin-orbit split doublet with a splitting of ~ 5 eV and broadened with many, unresolved contributions from individual multiplets. The features at E_{rel} = ~15 and ~20 eV are not present. The two lower BE features predicted by the AMC theory are present with the correct E_{rel} and intensity. However, the smaller peak at E_{rel} = ~4 eV and the shoulder at E_{rel} = ~-1 eV are not accounted for.

In Fig. 8b, we include intra-atomic many-body effects as well as the AMC determinants. This inclusion leads to a small transfer of intensity from the lower E_{rel} portion of the spin-orbit split doublet to the higher E_{rel} part. The features missing from the AMC treatment are still missing when these additional many-body terms are included. In order to keep the size of the CI Hamiltonian matrix from growing too large, we do not consider these atomic many-body effects further. In Figs. 8c and 8d, we show the effect of adding the single and double shake kind of excitations to the AMC many-body effects. From Fig. 8d, where both single and double shake excitations are included, the features at E_{rel} = ~15 and ~20 eV are now well described and these features are clearly shake satellites. However, the features at lower BE, $E_{rel} \lesssim 10$ eV, are essentially unchanged for all levels of many-body theory we have considered thus far. Moreover, the features at E_{rel} = ~+4 and -1 eV are missing in all cases. Clearly, something is missing from our theoretical model.

The missing physics could be screening of the 2p core-hole by electrons in the Ti_2O_3 CB. Since Ti_2O_3 is a semiconductor at room temperature with a rather high carrier concentration as measured by the Hall effect ($\sim 10^{20}$ cm^{-3}), it is possible that this CB screening could interact with the localized open-shell multiplets for the ionized Ti center. This effect, clearly not considered with our embedded TiO_6 cluster model because only one Ti cation is treated quantum mechanically, might lead to a redistribution of intensity within the main doublet which could introduce the features missing in theory. This proposal can be regarded as an extension to the nonlocal screening proposed by Sawatzky *et al*. [22-23, 37] where the CB, "nonlocal" screening may be especially important for Ti_2O_3 because of the higher carrier concentration compared to the systems considered in their work. It is appropriate to ask why this CB nonlocal screening should be important for the 2p but not for the 3p core level. In section III.D, the screening of the core-hole for the Ti 2p and 3p configurations is considered and shown to be quite different. Indeed, the 2p hole is "over-screened" by a major increase in covalent mixing between the Fe 3d and O 2p when a core-hole is present. If the CB nonlocal screening reduces the covalent character for the 2p hole, and leads to more nearly pure 3d character in the local open-shell orbitals, this effect might account for the missing intensity in theory. More specifically, this effect could broaden and redistribute intensity for the AMC multiplets [35] and, possibly, lead to the missing features. This effect may be less important for the 3p spectrum since local screening did not over-screen the 3p core hole. This idea can be tested by including next-nearest Ti neighbors in the cluster model to form an embedded TiO_6Ti_{18} cluster [18]. Here nonlocal screening might naturally be included. Calculations with larger cluster models where the nonlocal screening can be taken into account constitute an entirely new set of calculations and are outside the scope of the present paper.

D. Electronic Structure of Ti_2O_3: Covalency and Screening

The covalent character of metal-ligand bonds is useful for understanding the properties of nominally ionic systems such as halides and oxides [38-39]. However, commonly used methods to characterize occupations of orbitals, especially Mulliken population analyses [40], have uncertainties. We have thus developed alternative methods to obtain quantitative estimates of covalent character [12, 25]. In particular, for the contracted 3d orbitals of first-row transition metal oxides, methods based on the projection of the atomic 3d orbitals onto cluster model wavefunctions, provide reliable estimates of their occupations. We denote these occupations in the orbital and total wavefunctions as $N_P(3d)$ [4, 25]. In Table I, we give information on the projected occupations and the open-shell 3d orbital energies for our cluster model of the ground state configuration of Ti_2O_3 with all core levels filled. For the closed-shell orbitals, we give the total 3d projection; in the absence of covalency this quantity is identically zero. The relative orbital energies ($\Delta\varepsilon$) as well as the 3d projections are also given in Table 1 for the ligand field and spin-orbit split open-shell orbitals. In the absence of covalency, the projection for these orbitals is unity. We also give the orbital size,[12, 25] denoted $<r>_{avg} = [<r^2>]^{1/2}$, as a further indication of covalent character. As the extent of mixing between O 2p and Ti 3d orbitals increases, the value of $<r>_{avg}$ becomes larger.

Several important features are clear from Table I. First, the rhombohedral symmetry of Ti_2O_3 breaks the degeneracies of the three low-lying, dominantly t_{2g}, orbitals and the two higher, dominantly e_g, orbitals. This degeneracy breaking is driven primarily by ligand field splitting, with spin-orbit splitting making only a minor contribution. The t_{2g} derived orbitals have a small amount of covalent character, having only lost 6-7% of their pure 3d character. On the other hand, the two e_g derived orbitals have considerably more covalent character, being only 60% and 80% pure 3d, respectively. This difference is a direct consequence of the orientation of the 3d orbitals. The t_{2g} orbitals are oriented between the ligands, resulting in low covalency, whereas the e_g orbitals are oriented toward the ligands which favors covalent mixing [4]. The associated sizes of these open-shell orbitals ($<r>_{avg}$) are fully consistent with the indications of covalent mixing given by the projections. The t_{2g} orbitals with $<r>_{avg} = \sim 0.95$Å are ~25% larger than the 3d orbitals of the isolated the Ti(III) cation for which $<r>_{avg} = 0.74$Å. On the other hand, the two e_g derived, higher-lying, open-shell orbitals have considerably larger $<r>_{avg}$ values since they have much larger covalent mixing with O 2p. The closed-shell orbitals, which are largely centered on the O ligands, have significant amounts of Ti 3d character. Rather than consider the projection of the Ti 3d on individual closed shell orbitals, the total projection over all closed shell orbitals is taken. This approach is physically correct since the electron density and the total WF are invariant for a unitary transformation of the closed shell orbitals. The total 3d character in the closed shell space is $N_P(3d) = 1.02$. This shows that the fully occupied closed-shell orbitals that have dominantly O 2p character have significant covalent bonding character. Using the method of constrained variations [12], it is estimated that this covalent bonding contributes 2.0 eV to the stability of Ti_2O_3. The open-shell orbitals correspond to the ground and d-d excitation excited states of Ti_2O_3 [39], where only the lowest excited state formed with the t_{2g} orbital at $\Delta\varepsilon = 0.2$ eV will have significant Boltzmann occupation at room temperature.

Analogous information on the covalent character of the open-shell and closed-shell orbitals is given in Table II for configurations for which there is a hole in either the Ti 2p or 3p shell,. As for the ground-state configuration, the open-shell orbitals are in t_{2g} and e_g groups for which the degeneracies are perturbed by ligand field and spin-orbit splittings. The projections for Np(3d) show that the open-shell t_{2g} derived orbitals continue to have only limited covalent mixing with the ligands whereas the e_g derived orbitals have significantly larger covalent character. However, the most striking change comes for the covalent character of the closed-shell orbitals. While there was ~1 e^- of 3d character for the ground state configuration when the core shells were filled, the covalent character increases the electron count by almost 1 e^- such that $N_P(3d) = 1.97$ for a 3p hole. Likewise, covalency increases the electron count by more than 1 e^- such that $N_P(3d) = 2.24$ for a 2p hole. In physical terms, the increase in covalency acts to screen the core hole. Indeed, based on the measure of the closed-shell N_P value, the 2p hole is actually over-screened by the change in covalency. The large change in the closed-shell covalency and core hole screening have significant consequences for the intensities of the shake satellites [4]. The intensity lost by the multiplets of the Koopmans' configuration for the hole states to shake satellites depends directly on the overlap of the initial state and hole state orbitals. Since the covalency is significantly different between the closed-shell orbitals of the ground and hole states, one would expect much larger losses from the main peaks to shake satellites for Ti_2O_3 than for an isolated Ti(III) cation. Furthermore, based on the larger closed-shell covalent character of the 2p hole configuration relative to the 3p hole configuration (see the N_P in Table II), the loss to satellites is expected to be larger for the Ti 2p spectrum than for the 3p spectrum. In this context, it is worth noting that the relationship of covalent mixing to the energies and intensities of shake-up satellites depends on the difference between the covalent character of the initial ground-state configuration and the final core-hole configuration [13]. Furthermore, details of the contributions of individual shake-up excitations, especially into either the t_{2g} or e_g orbitals, is complex; this can easily be seen from the plots in Figs. 7 and 8 where it is clearly shown that many individual final states contribute to the Ti 2p and 3p spectra. Our objective here is to establish that the covalent contribution to the Ti-O interaction, especially for screening of the core-hole, is responsible for the satellite intensity; further details are beyond the scope of the present paper.

Using the sudden approximation for the core-level intensities, it is straightforward to calculate the intensity gain in the satellites and the associated intensity loss from the main multiplet peak manifold [4, 26]. The direct connection between covalent screening of the core hole discussed above is made by considering the losses from the main (i.e. Koopmans' theorem) configurations to CT satellites [4, 13]. In Table III, the intensity "losses" from the main peaks to the shake satellites for the 2p and 3p spectra are compared for the isolated Ti(III) cation and Ti_2O_3. The losses to satellites are much larger for Ti_2O_3 than for isolated Ti(III) since for the latter, the only contribution to shake intensity comes from contraction of the outer Ti orbitals due to the core hole. In contrast, the covalent screening of the core hole in Ti_2O_3 allows much more intensity to be lost to the satellites. Moreover, the losses to satellites are much larger for the 2p hole than for the 3p hole. This result is fully consistent with the larger closed-shell covalency for the 2p hole configuration as indicated by the projected 3d occupations (see Tables I and II). A consequence of the greater losses to shake satellites is that it may be more difficult to model the 2p than the 3p spectra.

IV. Conclusions

The core-level photoelectron spectra associated with structural Ti(III) in single-crystal Ti_2O_3 are rather complex. This complexity is due to final-state effects associated with angular momentum coupling, intra-atomic many-body effects, and core-hole screening including shake, or charge transfer, processes accompanying core photoionization. The core-hole screening may also include screening by conduction band electrons which are not included in our present local cluster model of Ti_2O_3. However, first-principles modeling without any adjustable parameters can capture much of this physics, depending on the size of the embedded cluster treated quantum mechanically.

Acknowledgements

The authors are indebted to Prof. Victor Henrich for providing the Ti_2O_3 single crystals. The PNNL work was supported by Laboratory Directed Research and Development funds and by the the U.S. Department of Energy, Office of Science, Division of Materials Sciences and Engineering under Award #10122 and was performed in the Environmental Molecular Sciences Laboratory, a national scientific user facility sponsored by the Department of Energy's Office of Biological and Environmental Research and located at PNNL. Battelle Memorial Institute operates PNNL for the USDOE under contract DE-AC05-76RL01830. P.S.B. was supported by the U.S. Department of Energy, Office of Science, Office of Basic Energy Sciences, Chemical Sciences, Geosciences, and Biosciences Division under the Geosciences program at PNNL. M.J.W., N.F.Q. and L.F.J.P. acknowledge support from the National Science Foundation under DMR 1409912. We thank Diamond Light Source for access to beamline I09 (NT16630) that contributed to the results presented here. We also thank beamline scientist Christoph Schlueter at the Diamond Light Source for his assistance.

References

1. G. Hollinger and F. J. Himpsel, Appl. Phys. Lett. **44**, 93 (1984).
2. P. S. Bagus, A. Wieckowski, and H. Freund, Comp. Theor. Chem. **987**, 22 (2012).
3. B. Richter, H. Kuhlenbeck, H. J. Freund, and P. S. Bagus, Phys. Rev. Lett. **93**, 026805 (2004).
4. P. S. Bagus, E. S. Ilton, and C. J. Nelin, Surf. Sci. Rep. **68**, 273 (2013).
5. W. R. Robinson, J. Sol. St. Chem. **9**, 255 (1974).
6. F. J. Morin, Phys. Rev. Lett. **3**, 34 (1959).
7. W. W. Yan, M. Fang, M. Liu, S. H. Kang, R. N. Wang, L. D. Zhang, and L. Liu, J. Appl. Phy. **111** (2012).
8. V. Singh and J. J. Pulikkotil, J. Alloys Comp. **658**, 430 (2016).
9. R. L. Kurtz and V. E. Henrich, Surf. Sci. Spectra **5** (1998).
10. Y. Z. Chen, N. Bovet, F. Trier, D. V. Christensen, F. M. Qu, N. H. Andersen, T. Kasama, W. Zhang, R. Giraud, J. Dufouleur, T. S. Jespersen, J. R. Sun, A. Smith, J. Nygard, L. Lu, B. Buchner, B. G. Shen, S. Linderoth, and N. Pryds, Nat. Comm. **4**, 2394 (2013).
11. P. Xu, Y. Ayino, C. Cheng, V. S. Pribiag, R. B. Comes, P. V. Sushko, S. A. Chambers, and B. Jalan, Phys. Rev. Lett. **117**, 106803 (2016).
12. P. S. Bagus, C. J. Nelin, D. A. Hrovat, and E. S. Ilton, J. Chem. Phys, **146**, 134706 (2017).
13. P. S. Bagus, C. J. Nelin, and E. S. Ilton, J. Chem. Phys, **139**, 244704 (2013).
14. J. M. Honig and T. B. Reed, Phys. Rev. **174**, 1020 (1968).
15. T. B. Reed, R. E. Fahey, and J. M. Honig, Mat. Res. Bull. **2**, 561 (1967).
16. L. Visscher, O. Visser, P. J. C. Aerts, H. Merenga, and W. C. Nieuwpoort, Comp. Phys. Comm. **81**, 120 (1994).
17. C. J. Ballhausen, *Introduction to Ligand Field Theory* (McGraw-Hill, New York, 1962).
18. C. J. Nelin, F. Uhl, V. Staemmler, P. S. Bagus, Y. Fujimori, M. Sterrer, H. Kuhlenbeck, and H.-J. Freund, Phys. Chem. Chem. Phys. **16**, 21953 (2014).
19. C. J. Nelin, P. S. Bagus, C. R. Brundle, E. S. Ilton, and K. M. Rosso, J. Chem. Phys, (to be submitted).
20. J. Q. Broughton and P. S. Bagus, Phys. Rev. **B 36**, 2813 (1987).
21. J. Q. Broughton and P. S. Bagus, Phys. Rev. **B 30**, 4761 (1984).
22. M. A. van Veenendaal and G. A. Sawatzky, Phys. Rev. Lett. **70**, 2459 (1993).
23. M. A. van Veenendaal, H. Eskes, and G. A. Sawatzky, Phys. Rev. **B**,**47**, 11462 (1993).
24. J. C. Slater, *Quantum Theory of Atomic Structure, Vols. I & II* (McGraw-Hill, New York, 1960).
25. P. S. Bagus and C. J. Nelin, J. Eectr. Spectrosc. Rel. Phenom. **194**, 37 (2014).
26. T. Aberg, Phy. Rev. **B 156**, 35 (1967).
27. P. O. Löwdin, Phys. Rev. **97**, 1474 (1955).
28. F. Prosser and S. Hagstrom, Intl. J. Quant. Chem. **2**, 89 (1968).
29. F. Prosser and S. Hagstrom, J. Chem. Phys. **48**, 4807 (1968).
30. J. A. Gubner, J. Phys. **A 27**, L745 (1994).

31. C. J. Nelin, P. S. Bagus, M. A. Brown, M. Sterrer, and H.-J. Freund, Angew. Chem. Intl. Ed. **50**, 10174 (2011).
32. DIRAC, *a relativistic ab initio electronic structure program, Release DIRAC08 (2008), written by L. Visscher, H. J. Aa. Jensen, and T. Saue, with new contributions from R. Bast, S. Dubillard, K. G. Dyall, U. Ekström, E. Eliav, T. Fleig, A. S. P. Gomes, T. U. Helgaker, J. Henriksson, M. Iliaš, Ch. R. Jacob, S. Knecht, P. Norman, J. Olsen, M. Pernpointner, K. Ruud, P. Sałek, and J. Sikkema (see the URL at* http://dirac.chem.sdu.dk. , 2008).
33. *CLIPS is a program system to compute ab initio SCF and correlated wavefunctions for polyatomic systems. It has been developed based on the publicly available programs in the ALCHEMY package from the IBM San Jose Research Laboratory by P. S. Bagus, B. Liu, A. D. McLean, and M. Yoshimine.*
34. P. S. Bagus, C. J. Nelin, S. A. Chambers, M. H. Engelhard, and L. Piper, (in preparation).
35. P. S. Bagus and E. S. Ilton, Phys. Rev. **B 73**, 155110 (2006).
36. A. J. Freeman, P. S. Bagus, and J. V. Mallow, Intl. J. Mag. **4**, 49 (1973).
37. D. Alders, F. C. Voogt, T. Hibma, and G. A. Sawatzky, Phys. Rev. **B** (Condensed Matter) **54**, 7716 (1996).
38. F. A. Cotton and G. Wilkenson, *Advanced Inorganic Chemistry* (Wiley, New york, 1972).
39. J. S. Griffith, *The Theory of Transition-Metal Ions* (Cambridge Press, Cambridge, 1971).
40. R. S. Mulliken, J. Chem. Phys. **23**, 2338 (1955).

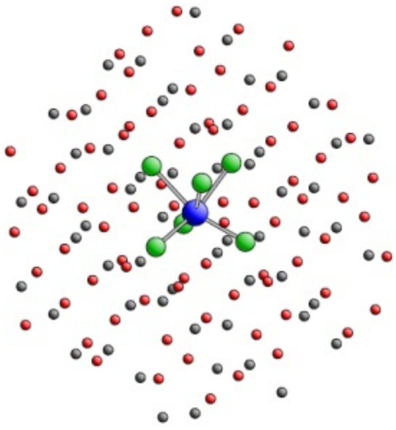

Fig. 1. Schematic view of the rhombohedral, embedded TiO_6 cluster to model Ti_2O_3. The central Ti atom and the 6 nearest neighbor O atoms are shown as large spheres. The embedding point charges, placed at lattice positions, are shown as small spheres.

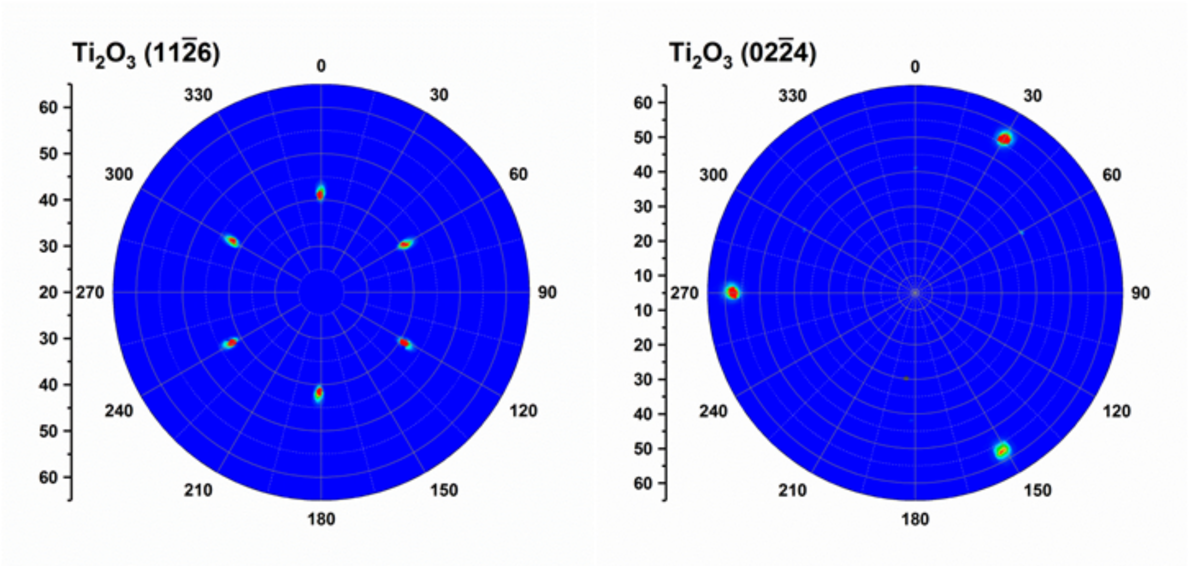

Fig. 2. Intensities of the $(11\bar{2}6)$ and $(02\bar{2}4)$ x-ray diffraction peaks plotted in polar coordinates. The radial axis indicates the angle of the scattering vector from a normal to the sample surface, while the circumferential axis indicates the angle of the in-plane component of the scattering vector relative to an arbitrary direction.

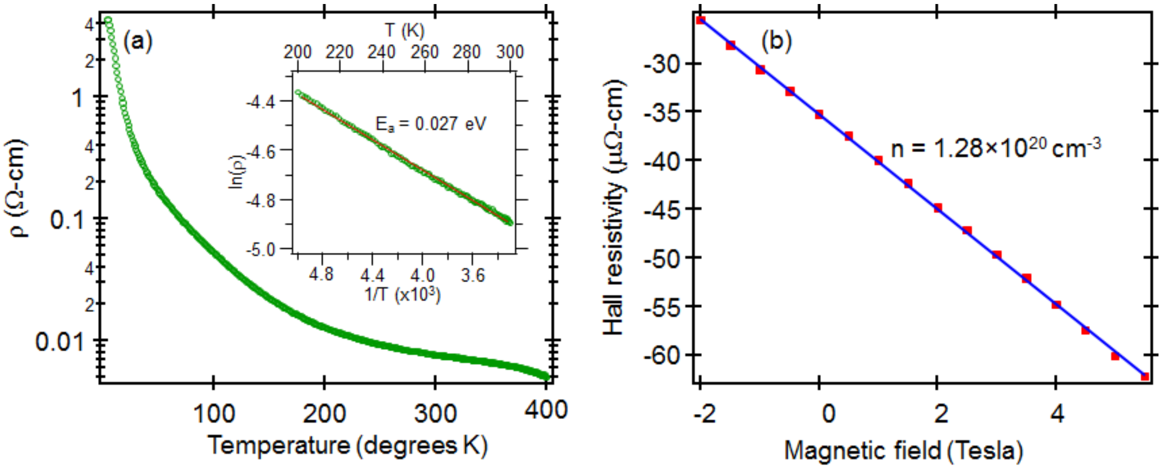

Fig. 3. ρ vs T (a) and Hall effect data measured at ambient temperature (b) for single crystal Ti_2O_3.

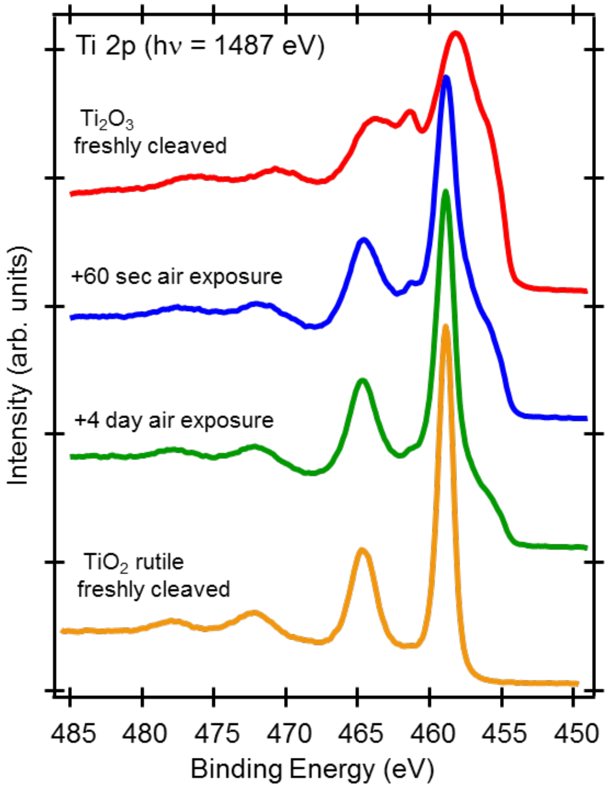

Fig. 4. Normal emission Ti 2p spectra for anoxically cleaved crystals of Ti_2O_3 (top) and TiO_2 rutile (bottom), along with spectra for cleaved Ti_2O_3 after controlled exposures to air (middle two), excited with AlKα x-rays (hν = 1487 eV). The spectrum for TiO_2 rutile after air exposure (not shown) is identical to that for the anoxically cleaved crystal.

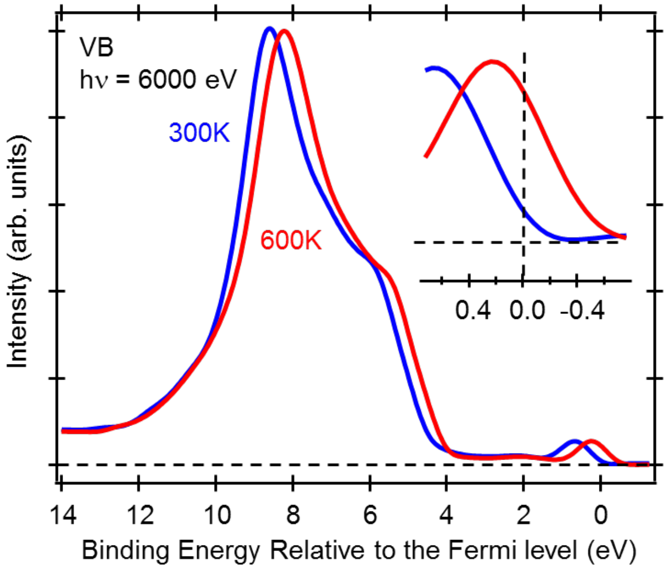

Fig. 5. Valence band spectra for anoxically cleaved Ti_2O_3 above and below the MIT excited with hard x-rays.

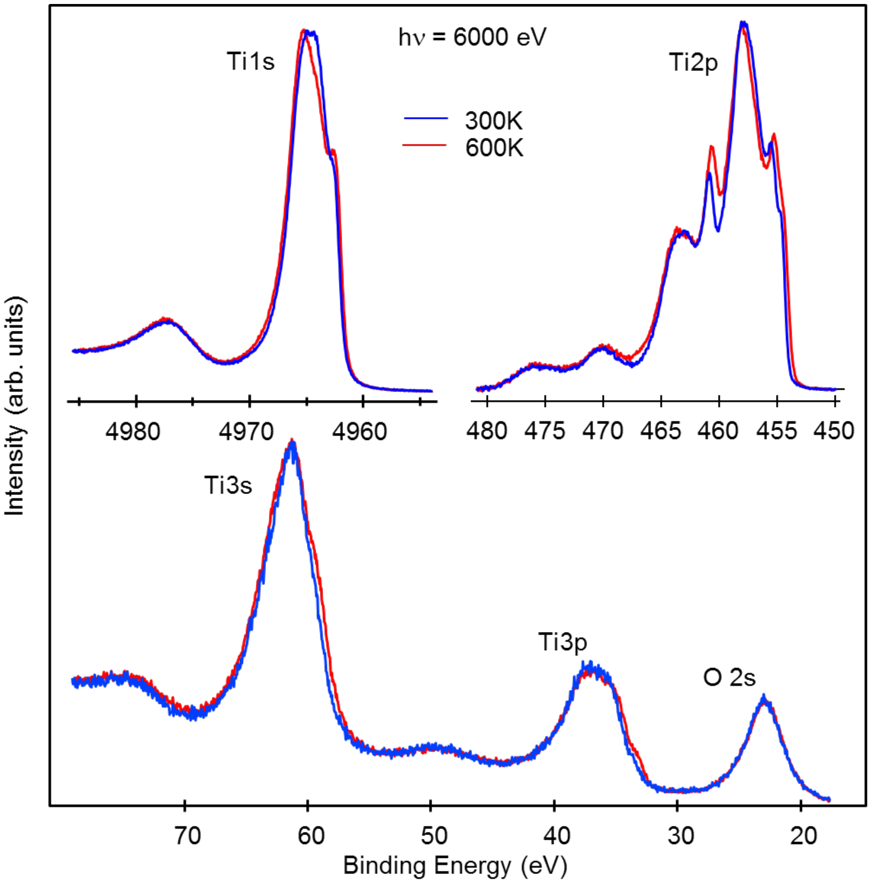

Fig. 6. Core-level spectra for anoxically cleaved Ti_2O_3 above and below the MIT excited with hard x-rays.

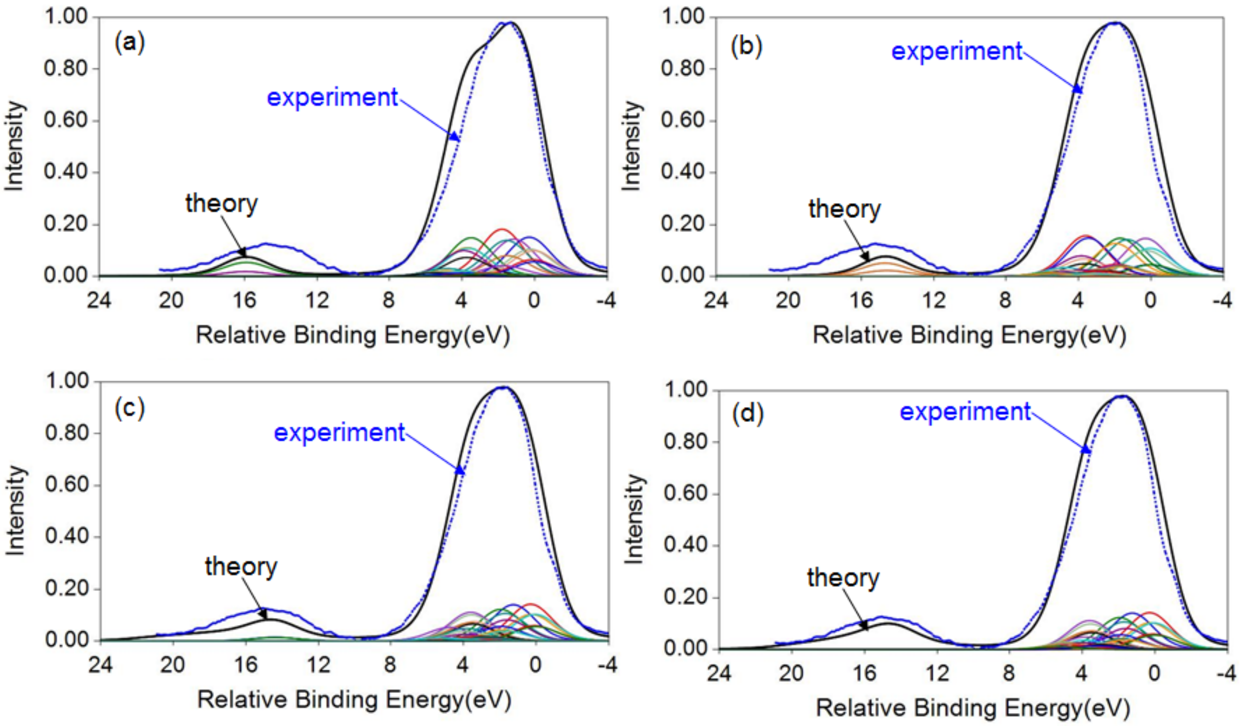

Fig. 7. Progression of DHF theory, along with experiment, for Ti 3p as different kinds of many-body interactions are included: (a) AMC only -- 60 determinants, (b) AMC plus intra-atomic many body -- 3720 determinants, (c) AMC plus intra-atomic and single-electron inter-atomic CT -- 5340 determinants, (d) AMC plus intra-atomic and single- and double-electron inter-atomic CT -- 8940 determinants. The light curves below the total solid curve for theory are for the most intense individual contributions. In addition to these, there are many other weaker contributions that, although not shown, constitute in aggregate a significant fraction of the total intensity.

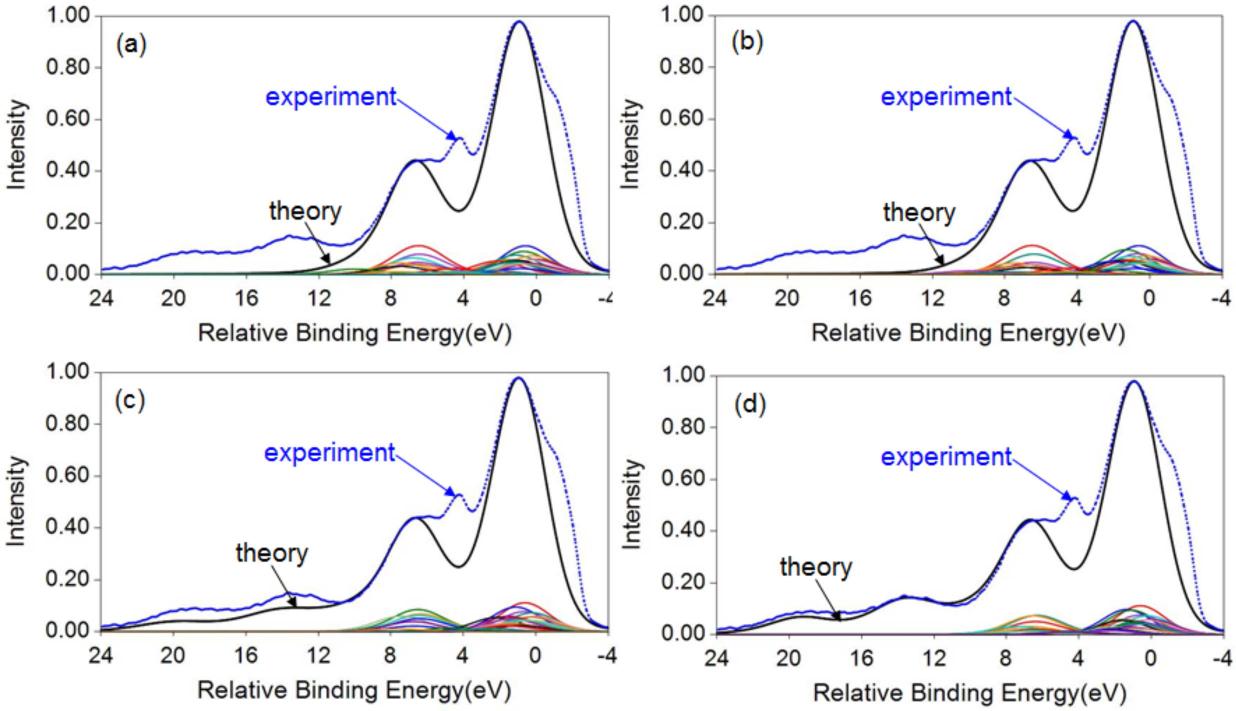

Fig. 8. Progression of DHF theory for Ti 2p, along with experiment, as different kinds of many-body interactions are included: (a) AMC only -- 60 determinants, (b) AMC plus intra-atomic many body – 12,120 determinants, (c) AMC plus intra-atomic and single-electron inter-atomic CT – 5,280 determinants, (d) AMC plus intra-atomic and single- and double-electron inter-atomic CT – 18,060 determinants. See caption to fig. 7 and text for a discussion of the individual contributions to the total theoretical XPS shown with light lines.

Table I. Changes in orbital energy with respect to the lowest orbital energy (Δε),projected Ti 3d characters on the open t_{2g} and e_g orbitals as well as on the closed shell orbitals (Np(3d)), and orbital sizes ($<r>_{avg}$) for the embedded TiO_6 cluster model of Ti_2O_3. The ligand field and spin-orbit split open-shell orbitals are described as being derived from the cubic (O_h), t_{2g} and e_g symmetries. For the closed-shell orbitals, the 3d character is summed over all closed orbitals, but the largest contribution is from orbitals that are dominantly O 2p.

	Δε (eV)	N_P(3d)	$<r>_{avg}$ (Å)
Open "t_{2g}"	0.00	0.93	0.97
Open "t_{2g}"	0.02	0.94	0.92
Open "t_{2g}"	0.28	0.93	0.95
Open "e_g"	1.48	0.59	1.86
Open "e_g"	1.77	0.78	1.22
Closed	-------	1.02	-------

Table II. Δε and N_P(3d), of the closed and open-shell orbitals for the 2p and 3p core hole configurations of Ti_2O_3; see caption to Table I.

	3p hole		2p hole	
	Δε (eV)	N_P(3d)	Δε (eV)	N_P(3d)
Open "t_{2g}"	0.00	0.93	0.00	0.91
Open "t_{2g}"	0.02	0.93	0.03	0.92
Open "t_{2g}"	0.27	0.91	0.25	0.89
Open "e_g"	1.98	0.73	1.94	0.67
Open "e_g"	2.11	0.71	2.08	0.65
Closed	-------	1.97	-------	2.24

Table III. Losses to shake satellites as a fraction of the total XPS intensity for the 2p and 3p spectra of Ti_2O_3; the losses are given separately for the *j* = 3/2 and *j* = 1/2 components.

	Ti 3p		Ti 2p	
	Ti^{3+}	Ti_2O_3	Ti^{3+}	Ti_2O_3
$2p_{3/2}$ losses	2.1%	14.3%	8.7%	25.3%
$2p_{1/2}$ losses	2.1%	14.1%	8.7%	25.3%